J. Fluid Mech. (1986), *vol.* 164, *pp.* 383–400
Printed in Great Britain

A boundary-integral method for two-phase displacement in Hele-Shaw cells

By A. J. DEGREGORIA AND L. W. SCHWARTZ

Corporate Research-Science Laboratories, Exxon Research and Engineering Co., Clinton Township, Route 22 E., Annandale, New Jersey 08801, USA

(Received 18 February 1985 and in revised form 13 August 1985)

We develop a time-dependent numerical algorithm, using a boundary-integral approach, to investigate fingering in Hele-Shaw cells. Starting from a sinusoidal variation in the initial interface, stable fingers quickly form for a wide range of the dimensionless surface-tension parameter. For very low values of the parameter, the incipient finger bifurcates. The stable fingers are clearly the same as those obtained by McLean & Saffman (1981) using a steady-state algorithm. These steady-state solutions were found to be linearly unstable. We resolve this apparent discrepancy regarding stability by tracing the fate of small disturbances placed on and about the finger tip. We show that some small disturbances do, indeed, grow initially; however, they reach a maximum amplitude and decay as they convect backward from the tip of the finger to regions where stabilizing surface tension is the major physical force. Relatively large imposed disturbances, on the other hand, cause a finger to bifurcate; the critical disturbance amplitude decreases as the surface tension is reduced,

1. Introduction

The 'fingering' phenomenon in Hele-Shaw cells has been investigated both experimentally and theoretically for the past quarter-century. Recently this interest has intensified because the phenomenon and the simplified equations that model it appear relevant to questions regarding two-phase displacement in oil reservoirs and more general investigations of pattern formation in 'noisy' systems. In both cases, the most relevant limit is when the stabilizing effect of surface tension is very small.

Saffman & Taylor (1958), in a classic paper, performed experiments displacing a viscous fluid from between two closely spaced plates, a Hele-Shaw cell, with a less viscous fluid. They point out an analogy between immiscible displacement in a Hele-Shaw cell and the equivalent problem in a two-dimensional idealization of a porous medium. In both cases, within a single-phase region of constant permeability, conservation of mass and the linear dependence of velocity on pressure gradient yield a potential-flow problem. The kinematic boundary condition, that particles on the moving interface remain there for all time, is also common to both problems. Potential differences between these problems derive from the pressure boundary condition on the moving front. In a Hele-Shaw cell, the idealized boundary condition is that the pressure jump across the front is proportional to the local curvature of the interface when the cell is viewed from above. This assumes that the interface curvature in the transverse direction, i.e. between the plates, is constant, an assumption that has been seriously questioned by Pitts (1980) and others. For porous-media flows, the situation is even less well understood. Experiments by Chouke, van Meurs & van der Poel (1959) and Peters & Flock (1981), using model

porous media, suggest that acceptable results for linear stability of a slightly perturbed plane interface can be obtained by assigning an effective surface tension to this interface, proportional to the actual surface tension. Recent theoretical studies by Jeraud, Davis & Scriven (1984) suggest that the effective-surface-tension viewpoint is an oversimplification. Their more detailed theory includes pore-scale effects and leads to different values for the most unstable and neutrally stable wavelengths. Neither viewpoint has as yet been extended to the nonlinear regime when the interface is grossly distorted.

Saffman & Taylor (1958) found that a single stable finger ultimately forms in the apparatus for a wide range of experimental conditions. The experiments of Pitts (1980) confirmed their result.

Taylor & Saffman (1959) performed a linear stability analysis on steady-state finger profiles for zero surface tension, finding that the fingers are linearly unstable. McLean & Saffman (1981) extended the analysis to include the effect of finite surface tension, finding that these fingers are also linearly unstable. For non-zero surface tension, the steady-state finger profiles are determined numerically, using Newton iteration.

There is an apparent contradiction between theory and experiment – theory indicates that fingers are unstable while experiment indicates stability. To complicate the situation, Romero (1982) numerically discovered multiple steady-state solutions for a range of values of the surface tension. Indeed, Vanden-Broeck (1983) showed that there is a countable infinity of such solutions. Linear stability analyses on these additional steady-state finger profiles have not been performed to our knowledge.

Within the context of more general studies, time-dependent calculations simulating the two-phase Hele-Shaw-cell experiments have been performed by Meng & Thomson (1978) and by Tryggvason & Aref (1983, 1985) using the 'vortex-in-cell' method. Starting with a sinusoidal variation in the interface with a wavelength equal to the channel width, Tryggvason & Aref calculate fingers that evolve to a steady profile in a finger-fixed reference frame. For relatively large surface tension, these ultimate profiles agree closely with the steady-state results of McLean & Saffman. These results appear to establish that, at least, some fingers are ultimately stable in the full nonlinear sense. The vortex-in-cell method employs a fixed rectangular grid; for this reason it is not well suited to address the stability issue for low values of surface tension where high resolution is vital.

In order to help resolve the stability issue, we present a time-dependent numerical algorithm based on an accurate boundary-integral approach. We find that stable steady-state fingers can be formed for a wide range of values of surface tension. These fingers are apparently those found by McLean & Saffman (1981) using their steady-state algorithm. We provide an explanation for the apparent discrepancy between our stable fingers and the linear instability found by McLean & Saffman. Tracing small disturbances with both the full nonlinear time-dependent model and a simplified 'linear' model, we show that some disturbances initially grow, reach a maximum, and then decay. The reason for the ultimate decay is that all disturbances convect backward, away from the finger tip, to the region where stabilizing surface tension becomes the dominant physical effect acting on the disturbance.

We find that, for very low values of the dimensionless surface tension, an incipient finger, rather than progressing toward a fully developed stable finger, flattens at the tip and splits. This bifurcation is the result of a nonlinear instability. Placing a recess at the tip of a developing stable finger, we show that, above a certain amplitude, the recess causes bifurcation. As dimensionless surface tension decreases the amplitude

needed for bifurcation decreases until it is within the range of 'numerical noise' that is associated with the discrete approximation of continuous functions.

Recently, branched structures have been observed in two-phase Hele-Shaw experiments by Park & Homsy (1985) and Nittmann, Daccord & Stanley (1985). The bifurcation we observe for very low surface tension may be the all-important step in this process. It is simple to show that when a finger bifurcates, the new situation of two fingers progressing up the channel side by side is also unstable. If one finger gets a little ahead of the other, it will suppress the growth of the other finger to the point where it effectively stops growing. (Saffman & Taylor 1958 observed this suppression experimentally during the initial stages of unstable displacement and it has been simulated numerically by Tryggvason & Aref 1983.) We now have a single finger progressing up the channel again and the situation can recur. From this mechanism we should expect a simple tree-like structure, where we have a main branch with single side branches at random locations on either side of the main branch. For extremely low surface tension, a finger may again bifurcate before being suppressed, so more complicated tree-like structures may also be possible. Further results, primarily focusing on the low-surface-tension limit, will be available in the near future.

Section 2 gives the basic equations and numerical method used in the fingering computations. The full equations and interfacial conditions for unsteady three-dimensional viscous flow of two immiscible fluids are given in Wehausen & Laitone (1960, p. 453 *et seq.*). Since the exact problem as posed is effectively intractable, we consider here the 'standard' simplified problem as formulated by previous workers (with the notable exception of Pitts 1980). A partial statement of the simplifying assumptions leading to these 'Hele-Shaw equations' may be found in Tryggvason & Aref (1983). See also the recent work of Park & Homsy (1984). It is important to remember that the Hele-Shaw equations do not correctly predict the experimentally observed ratio of developed finger width to channel width and the reason for the discrepancy is not well understood. When surface tension is small, however, both experiment and theory obtain values of this ratio that are close to 0.5.

In §3 we present numerical results for the growth of an imposed initial disturbance on a flat interface. For a range of values of surface tension these disturbances become steady-state fingers whose widths are in close agreement with the calculations of McLean & Saffman (1981). The effect of perturbations of these developed fingers is then explored. Two distinct effects are observed: either the disturbance ultimately decays after some period of growth, or the disturbance causes the finger to bifurcate at its tip.

A heuristic model of disturbance growth is presented in §4. For small surface tension, a perturbation is idealized as a localized pulse that passively convects backward along a developed finger. As it moves, its Fourier spectrum is altered using a local-stability argument. The resulting growth and decay are qualitatively similar to our numerical results and the apparent contradiction between predicted instability and observed stability may thus be better understood. Our simplified model is somewhat similar to the amplitude-ratio methods discussed by Reshotko (1976) in his survey of boundary-layer stability.

Results of the present study are summarized in §5.

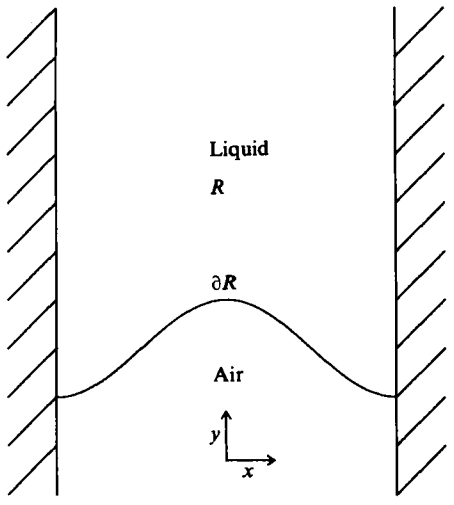

FIGURE 1. Sketch of the Hele-Shaw cell.

2. Equations and numerical method

We assume a cell of infinite length in which air is pushing a liquid, as shown in figure 1. The pressure in the air is a constant, which we may take to be zero. The pressure p in the liquid, region R, is a function of the spatial coordinates x and y. Since the plate spacing is assumed to be small compared with other lengths in the problem, we have 2-dimensional Poiseuille flow locally, in the liquid, yielding the following relationship between the depth-averaged velocity and the pressure gradient:

$$\bar{v} = -M\nabla p, \quad M = \frac{b^2}{12\mu}, \tag{1}$$

where b is the plate spacing and μ is the liquid viscosity. Assuming the liquid to be incompressible, the continuity equation is

$$\nabla \cdot \bar{v} = 0. \tag{2}$$

Combining the two equations, we obtain Laplace's equation for the pressure in the liquid:

$$\nabla^2 p = 0. \tag{3}$$

At the air–liquid boundary, denoted by ∂R in the figure, the pressure on the liquid side is augmented by surface tension from its value of zero on the air side by the expression

$$p(x,y) = \sigma \frac{\mathrm{d}\theta}{\mathrm{d}s} \quad ((x,y) \in \partial R). \tag{4a}$$

where s is the arclength along the surface, measured from some reference point, θ is the angle the tangent to the surface makes, with respect to some reference direction, and σ is the surface tension. Viewed from the liquid, p is positive at any point where the surface is concave.

On the moving interface ∂R the kinematic boundary condition, that a particle on this boundary remain on the boundary for all time, must also be satisfied. Restated, this condition is that the normal component of fluid velocity, with Cartesian

components (u, v), of a particle occupying a point on the surface, is equal to the normal component of the surface velocity (x_t, y_t) at that point. Thus

$$(u, v)\cdot\bar{n} = (x_t, y_t)\cdot\bar{n} \quad ((x, y)\in\partial R), \tag{4b}$$

where $\bar{n}$ is a normal vector to ∂R and subscripts signify time differentiation. Because Hele-Shaw flow is a subset of creeping motion, inertial contributions to the interface motion are neglected and surface velocity components, found by solving (3) at each instant of time, yield the instantaneous surface motion according to (4*b*).

On the sidewalls of the cell, the normal component of fluid velocity is zero, i.e.

$$\frac{\partial p}{\partial x} = 0 \quad (x = \pm\tfrac{1}{2}L), \tag{5}$$

where L is the channel width. The no-slip boundary condition for viscous flow cannot be imposed within the framework of the Hele-Shaw model.

At upstream infinity we assume constant velocity,

$$M\nabla p \to -\frac{Q}{bL}\bar{y} \quad (y\to+\infty), \tag{6}$$

where Q is the volumetric flow rate into the channel and $\bar{y}$ is a unit vector in the direction of increasing y.

Transforming to dimensionless length, pressure and velocity,

$$x' = \frac{x}{L}, \quad y' = \frac{y}{L}, \quad p' = \frac{Mb}{Q}p, \quad v' = \frac{bL}{Q}v, \tag{7}$$

we have the following equations and boundary conditions for the liquid:

$$\bar{v} = -\nabla p \qquad ((x, y)\in R); \tag{8}$$

$$\nabla^2 p = 0 \qquad ((x, y)\in R); \tag{9}$$

$$\frac{\partial p}{\partial x} = 0 \qquad (x = \pm\tfrac{1}{2}); \tag{10a}$$

$$\nabla p \to \bar{y} \qquad (y\to+\infty); \tag{10b}$$

$$p = \frac{\sigma Mb}{QL}\frac{\mathrm{d}\theta}{\mathrm{d}s} \quad \text{on } \partial R; \tag{10c}$$

where we have dropped the primes. The kinematic boundary condition (4*b*) remains unchanged, where, using (7), the time is measured in units of bL^2/Q. The only parameter we have is the 'dimensionless surface tension'

$$\tau = \frac{\sigma Mb}{QL}. \tag{11}$$

Because the liquid domain R in the $(z = x+\mathrm{i}y)$-plane is semi-infinite, Laplace's equation will be solved in the transformed $(\zeta = \xi+\mathrm{i}\eta)$-plane. The conformal map

$$\zeta = \mathrm{e}^{2\pi\mathrm{i}z}$$

takes the unit sink at upstream infinity into a unit sink at the origin in the ζ-plane. The moving boundary $\partial R(t)$ maps to the closed curve surrounding the origin $\partial R_\zeta(t)$. The liquid region R maps onto the annular region R_ζ bounded by ∂R_ζ and a small circle enclosing the origin and, because the flow is assumed to be bilaterally symmetric

about the channel centreline in the z-plane, the complex velocity $\mathrm{d}f/\mathrm{d}\zeta$ is analytic within that annulus. Numerical values of the complex potential $f = p + \mathrm{i}\psi$ are unaffected by the mapping.

At any point within or upon ∂R_ζ, the complex potential is given by the superposition of contributions from the unit sink at the origin and distributed sources on ∂R_ζ, i.e.

$$f(\zeta) = -\frac{1}{2\pi}\ln\zeta + \frac{1}{2\pi}\int_{\partial R_\zeta} q(s_1)\ln(\zeta-\zeta_1)\,\mathrm{d}s_1. \tag{12}$$

The source line density q is a real function to be determined as part of the solution. Here s_1 may be taken as arclength on ∂R_ζ. With $p = \mathrm{Re}\{f\}$ given by (12), the integral equation for the source density is

$$\int_{\partial R_\zeta} q(s_1)\ln|\zeta-\zeta_1|\,\mathrm{d}s_1 = 2\pi p(s) - \ln|\zeta| \quad (\zeta\in\partial R_\zeta), \tag{13a}$$

where vertical bars denote the modulus of a complex number. Having determined q, the induced velocity at a point ζ, approaching ∂R_ζ from within, is given by

$$\frac{\mathrm{d}f}{\mathrm{d}\zeta} = u^{(\zeta)} - \mathrm{i}v^{(\zeta)} = -\frac{1}{2\pi\zeta} + \frac{1}{2\pi}\int\frac{q(s_1)}{\zeta-\zeta_1}\,\mathrm{d}s_1 - \mathrm{i}\,\frac{q(s)}{2}\,\mathrm{e}^{-\mathrm{i}\beta}. \tag{13b}$$

Here β is the inclination of a segment of ∂R_ζ measured counterclockwise from the direction of increasing $Re\{\zeta\}$. The integral is of Cauchy-principal-value type and the last term is the local contribution to the velocity which is most easily obtained using Gauss' theorem. The boundary-integral formulation in (13) can be shown to be equivalent to a method based on Green's formula; this relationship and the relevant existence proofs are discussed by Jaswon & Symm (1977, chap. IV).

We choose to march the solution in time using a full Lagrangian description, i.e.

$$\frac{\mathrm{d}\zeta}{\mathrm{d}t} = \frac{\mathrm{d}f}{\mathrm{d}\zeta} \quad (\zeta\in\partial R_\zeta). \tag{14a}$$

Finally, the velocities are transformed back to the z-plane by

$$\frac{\mathrm{d}z}{\mathrm{d}t} = \frac{\mathrm{d}f}{\mathrm{d}z} = \frac{\mathrm{d}f}{\mathrm{d}\zeta}\frac{\mathrm{d}\zeta}{\mathrm{d}t} \quad (z\in\partial R). \tag{14b}$$

Note that, from (4b), only the normal component of (14) need be satisfied. The full Lagrangian description allows us to monitor the surface dilation, which is sometimes also of interest.

The numerical solution is accomplished by representing the free surface in the z-plane by a set of $2N+1$ points or nodes. At any instant of time, the potential p at these nodes is calculated using a discrete version of condition (10c). After mapping the nodes to the ζ-plane, the potentials at the midpoints, between the nodes, are determined by interpolation. The source distribution is taken to be piecewise constant and the integrals in (13) are discretized, under this assumption, using formulas derived by Botha & Pinder (1983, §4.6). The resulting linear system for the source distribution from (13a) is solved and the ζ-plane velocities are calculated from (13b). After interpolation back to the nodes, the velocities are transformed to the z-plane using (14b). Note that, because of the assumption that the surface is bilaterally symmetric in the z-plane, and hence in the ζ-plane as well, the linear system to be solved is only of dimension N.

Given the node positions at any time and finding the corresponding particle

velocities by the above procedure, the surface evolution reduces to the solution of a coupled system of first-order nonlinear ordinary differential equations. Since the problem becomes stiff for higher values of the dimensionless surface-tension parameter τ, we have implemented a software package that has an option for solving stiff ordinary differential equations (ODE's), LSODE (Hindmarsh 1980), finding it efficient, accurate and easy to use in this application.

Particularly at low values of τ, velocities at the surface of the moving boundary are essentially normal to the surface. Node points, at the tip of a finger propagating into the liquid, take trajectories which quickly make the spacing large near the finger tip. To maintain good coverage at the tip, we redistribute points along a cubic-spline representation of the interface at regular intervals in time. In performing the redistribution, we place more points at places of high curvature by having the grid spacing Δs inversely proportional to a linear function of the curvature

$$\Delta s \propto \left(1 + c\left|\frac{\partial \theta}{\partial s}\right|\right)^{-1}, \tag{15}$$

where c is a constant.

Since we wish to address the question of stability with the time-dependent computations, we must have sufficiently fine grid spacing to depict all potentially unstable modes. If the interface is flat and infinite, we have the following results from a linear stability analysis (Saffman & Taylor 1958, Chouke *et al.* 1959):

$$l_{\mathrm{cr}}/L = 2\pi\tau^{\frac{1}{2}}; \tag{16}$$

$$l_{\max}/L = 2\pi\,(3\tau)^{\frac{1}{2}}; \tag{17}$$

where l_{cr} refers to the critical wavelength below which modes are stable, and $l_{\max}$ refers to the wavelength of maximum growth rate. The maximum grid spacing which can adequately describe a given sinusoidal disturbance is about one quarter the wavelength. We therefore can write the following inequality for the grid spacing needed to describe the evolution of a flat interface:

$$\Delta s_{\max} < 0.5\pi\tau^{\frac{1}{2}}, \tag{18}$$

where Δs is measured in units of the channel width L. As the evolving surface deviates significantly from flat, we use local conditions to determine the maximum local grid spacing

$$\Delta s_{\max} < 0.5\pi(\tau/u)^{\frac{1}{2}}. \tag{19}$$

Here, u is the local interface velocity in units of Q/bL.

Unless otherwise stated, the computations used $N = 50$, which is sufficient to satisfy inequality (19). A finer spacing was sometimes used to ensure convergence. The constant c in (15) is taken to be one.

3. Results of the computations

In this paper, we wish to focus on whether a single stable finger can be formed, particularly at low values of τ. To speed up the development of a single finger, we therefore impose a sinusoidal variation in the position of the initial interface in the time-dependent computations. The wavelength of the sinusoid is one, the channel width; the phase is chosen so that the peak is at the centre of the channel; and the amplitude is 0.05 for the computations shown here.

Figure 2 shows results of the time-dependent computations for a wide range of the

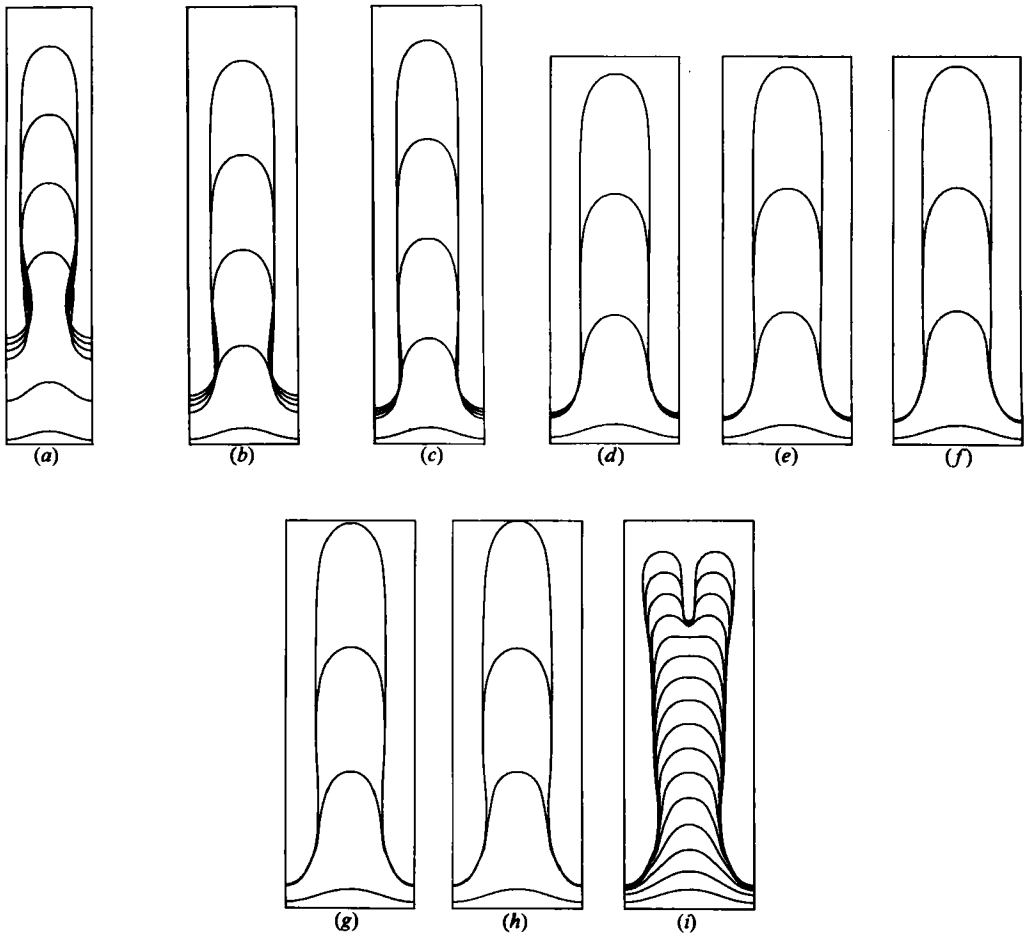

FIGURE 2. The computed time-evolution of an interface with an imposed sinusoidal variation of amplitude 0.05 (lowest curve), for different values of τ. The interface curves are shown at time intervals of 0.5. (*a*) $\tau = 0.02$, (*b*) 0.008, (*c*) 0.004, (*d*) 0.002, (*e*) 0.001, (*f*) 0.0005, (*g*) 0.0003 (*h*) 0.000 25, (*i*) 0.000 225.

surface-tension parameter τ. For all but the lowest value of τ shown, the initial small-amplitude sine wave quickly grows to form a stable finger. For high values of τ, the troughs that are formed move upward, perceptibly, and tend to round out, while, for low values of τ, the troughs, once formed, are essentially stagnant. It is easy to show, from the linear stability analysis, that, for $\tau = 0.0253$, the initial small-amplitude sine wave would be neutrally stable. We have verified this with the nonlinear time-dependent computations. For values of τ above this critical value, the small-amplitude initial sine wave decays. We cannot, therefore, generate stable fingers for $\tau > 0.0253$, by this method.

In figure 3, we show the asymptotic value of finger width λ for various values of the control parameter τ. Our results (triangles) are compared with results of Tryggvason & Aref (1985), given by circles and crosses, and the steady-state McLean & Saffman calculations (solid curve). In order to simplify direct comparison of these results, the control parameter is taken as $l_{\max}/L$, related to τ by (17), since

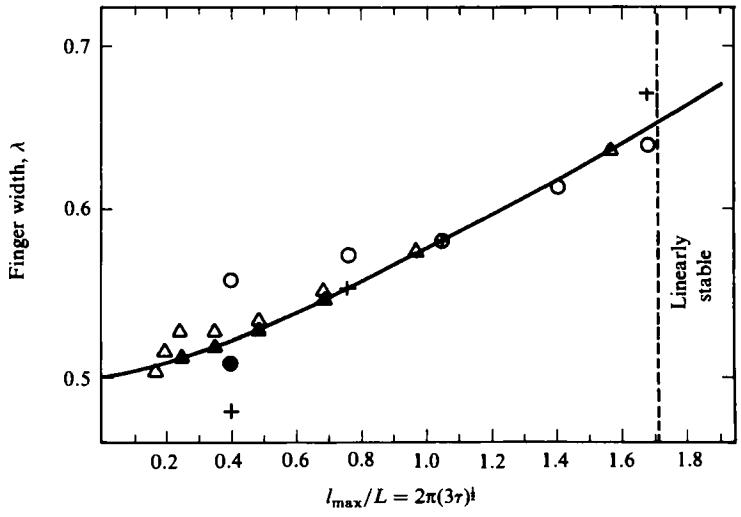

FIGURE 3. Variation of ultimate values of finger width λ with τ. The solid line is the steady-state computations of McLean & Saffman (1981); triangles denote time-dependent results from this study; circles and crosses are time-dependent results of Tryggvason & Aref (1985).

Tryggvason & Aref choose this format to present their points. Our values of τ range between 0.00025 and 0.02 corresponding to values of l_{max}/L between 0.172 and 1.534.

For the time-dependent calculations, it is necessary to state explicitly the criteria used to establish limiting values of λ. At steady-state conditions, mass conservation yields $u_1 \lambda = 1$, where u_1 is the translational speed of the finger. In the time-dependent results, as λ approaches its limiting value, the speed at the finger tip must also reach a limit, as given by this simple relation. Our data (triangles) are calculated as the limiting value of the tip speed, i.e. the surface velocity on the channel centreline. In all cases shown, finger widths correspond to three-decimal-place convergence as the finger progresses down the channel.

Various input parameters influence the asymptotic values of λ. Specifically we monitor, by repeated runs at the same value of τ, the rate of convergence of λ with time, the accuracy of the time-stepping calculations, the number of points used to represent the profile, and the time intervals at which the points are redistributed. The first two criteria may be dismissed most simply. Three-place convergence of λ with time was achieved in all cases shown in less than 1.5 time units, although the rate of convergence decreased as τ was reduced. The LSODE package used for the time integration allows the user to specify an error tolerance; this tolerance was always set at the level required to make negligible the potential errors arising from this integration. Because the interface dilates strongly at the tip, the last two control parameters are interrelated. For the points represented by open triangles in figure 3, 50 points per half-channel width were used. This was always sufficient to satisfy the criterion of four points per unstable wavelength, using local conditions, and the time interval between point redistribution Δt_s was taken as 0.05.

Particularly for the small values of τ, the values of λ were still somewhat sensitive to the choice of Δt_s and the number of points used to describe the profile. For all λ, convergence in Δt_s is obtained using a value of 0.0125. Decreasing this parameter costs little in computation time. To test convergence with the number of grid points, we

$\tau \backslash n$	8	16	32
0.0005	splits	0.510 (79)	—
0.001	0.529 (33)	0.521 (59)	—
0.002	0.543 (26)	0.533 (46)	0.530 (81)
0.004	0.566 (21)	0.551 (35)	0.547 (65)

TABLE 1. Finger width at various values of τ for different values of n, the number of grid points per local critical unstable wavelength. Numbers in parentheses are the total number of grid points on the surface.

introduce a point-redistribution scheme that is somewhat different from the procedure described in §2. Points are redistributed along the surface with a local spacing given by

$$\Delta s = \min\left(\frac{2\pi(\tau/u)^{\frac{1}{2}}}{n}, 0.5\left|\frac{\partial\theta}{\partial s}\right|^{-1}\right),$$

where u is the local interface speed in the normal direction, and n is the number of grid points per local neutrally stable wavelength, the latter being given by (16). Using this new criterion, the number of points used to represent the profile increases as the finger grows.

Table 1 gives λ as a function of n for values of τ of 0.0005, 0.001, 0.002 and 0.004 ($l_{\max}/L = 0.243$, 0.344, 0.487 and 0.688). Convergence from above is suggested with a convergence rate going approximately like $1/N^2$, where N is the total number of grid points. In the figure the solid triangles represent the values of λ obtained from table 1 using the largest value of n for which computations were performed at each τ-value. There is seen to be good correlation with the McLean & Saffman curve.

For comparison, the results of Tryggvason & Aref (1985) are shown as open circles, solid circles and crosses, corresponding to 8, 16 and 32 grid spacings per channel width respectively. Their vortex-in-cell technique works well for values of $l_{\max}/L$ in excess of 0.8; however, for $l_{\max}/L = 0.4$, the smallest value for which they present results, their contention that the solution has a λ-value significantly smaller than the McLean–Saffman result is not supported by our calculations. Even for their finest rectangular grid, resolution in the critical finger-tip region is very much less than that of the boundary-integral method with periodic point redistribution. Figure 4 illustrates this by showing the point distribution of the steady-state finger for $\tau = 0.0005$ and $n = 16$. Conversely, the vortex-in-cell method may well be the algorithm of choice for larger values of τ, especially when the interface is highly convoluted.

In figure 5 we show the evolution of an interface with a sinusoidal variation, for the same parameters as those in figure 2(*b*). We show the evolution for a longer time to establish that a steady state has indeed developed. We have run this simulation, for more than twice the time shown in figure 4, with no change in the result. The value of τ of 0.008 is the value at which the channel width equals the wavelength of maximum linear growth (see (17)).

Figure 2(*i*) illustrates a very interesting phenomenon when we attempt to grow a steady-state finger for the very low value of τ of 0.000225. The incipient finger, rather than taking the path to steady state, flattens at the tip and splits in two. This finger bifurcation was observed by Paterson (1981) in circular-Hele-Shaw-cell

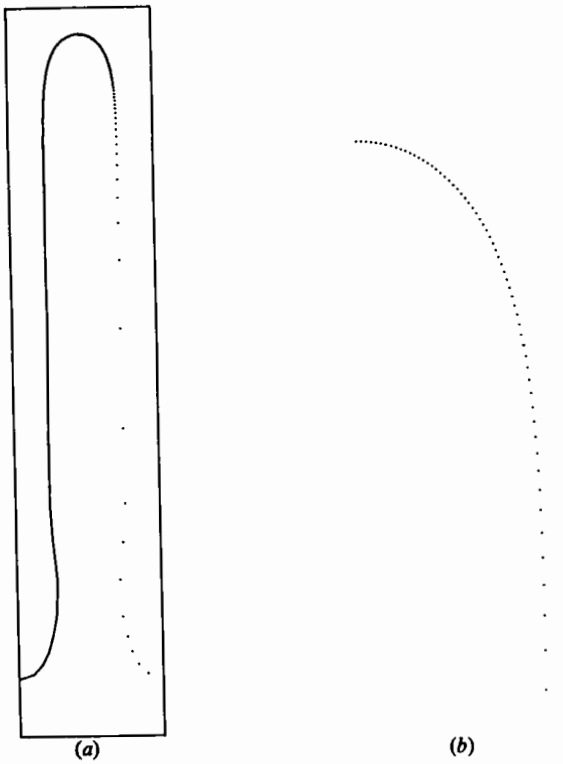

FIGURE 4. (*a*) High-accuracy computation of a steady-state finger at $\tau = 0.0005$ ($\lambda = 0.510$) illustrating the grid-point distribution. (*b*) The point distribution about the tip magnified 5 times.

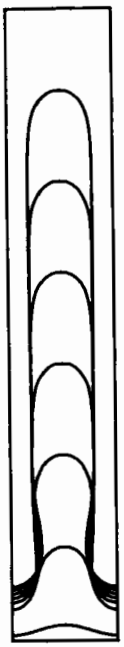

FIGURE 5. The same as figure 2(*b*) except the computation is shown for a longer time, indicating that a true steady-state finger has been formed.

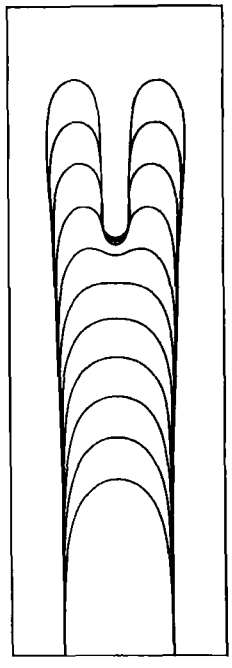

FIGURE 6. The effect of an instantaneously imposed recess of very small amplitude on the subsequent development of a finger, indicating that the fingers are linearly stable but nonlinearly unstable. The interface curves are presented at time intervals of 0.1.

experiments. (We have also simulated the circular geometry numerically and we observe finger bifurcation. These results will appear in a later paper.)

We conjecture that the splitting occurs because the fingers, for arbitrary τ, are nonlinearly unstable, i.e. developed fingers may well be stable to infinitesimal disturbances for all finite values of τ; however if sufficient noise is present the finger will split at or near the tip. This critical noise level decreases as τ is reduced. The numerical noise in our algorithm is sufficient, for the case shown in figure 2 (*i*), to cause tip splitting.

To demonstrate that fingers are nonlinearly unstable, we introduce a small-amplitude recess at the tip of the developed stable finger in figure 4 ($\tau = 0.0005$, time $t = 2.0$) and trace the subsequent evolution in figure 6. The recess can be described as follows:

$$(\Delta x, \Delta y) = A \cos(2\pi s/l_{\rm cr})\,(n_x, n_y) \quad (|s| < \tfrac{1}{4} l_{\rm cr}),$$
$$= 0 \quad (|s| \geqslant \tfrac{1}{4} l_{\rm cr}),$$

where A is the amplitude of the disturbance, (n_x, n_y) is the outward normal to the finger profile, $l_{\rm cr}$ is the local critical unstable wavelength at the finger tip, and s is the arclength. The arclength is taken to be zero at $x = 0$, the finger tip, and is positive when x is positive. The disturbance amplitude A is -0.000225 in figure 6. As we see in the figure, this very small disturbance is sufficient to cause the finger to bifurcate. Conversely, a disturbance with an amplitude of -0.0002 gives an evolution in which the finger does not bifurcate. The finger first fattens and then necks down, ultimately returning to its steady-state shape. Thus, we demonstrate that finger bifurcation, for this value of τ, is a nonlinear instability in which a disturbance must be of sufficient

τ	Critical amplitude
0.0005	0.00021
0.001	0.00213
0.002	0.0156

TABLE 2. The critical amplitude for instability for different values of τ. The uncertainty is less than 5%.

amplitude to cause the splitting. In table 2, we list values of the critical amplitude for bifurcation for three different values of τ, determined to within 5% by a binary search. As we can see from the table, the critical amplitude drops dramatically with τ, decreasing by about an order of magnitude as τ decreases by a factor of 2. We will examine finger stability in more detail in the next section.

4. A model stability analysis

A simplified model may be constructed that exhibits the basic features leading to bounded growth of a small-amplitude disturbance. It is an heuristic model that assumes localized disturbances that are passively convected backward with the local particle velocity. For small values of the surface-tension parameter τ, the shape of a developed finger is closely approximated by the Saffman–Taylor solution for $\tau = 0$ and $\lambda = \frac{1}{2}$,

$$e^{2\pi x} = \cos 2\pi y, \tag{20}$$

in a tip-fixed coordinate system. The arclength s, measured from the tip, is given by

$$\tanh 2\pi s = \sin 2\pi y. \tag{21}$$

The surface normal at a point s is at an angle θ with respect to the oncoming stream whose velocity is U. Because the potential is approximately constant for $\tau \ll 1$, the induced velocity of the singularity distribution is essentially normal to the interface. Thus the particle velocity of the liquid, at the interface, is given by

$$u_s = U \sin\theta = U \tanh 2\pi s \tag{22}$$

and U is equal to 2 in dimensionless units for $\lambda = \frac{1}{2}$.

We now consider a localized disturbance of small amplitude that is passively convected, from its initial position s_1 at time $t = 0$, backward along the finger with the particle velocity u_s. Assuming that its breadth is small compared to the local radius of curvature, the disturbance will 'see' an essentially constant normal velocity given by

$$u_n = U \cos\theta = \frac{U}{\cosh 2\pi s}. \tag{23}$$

We identify u_n with the destabilizing velocity in the stability calculation for a plane interface translating at constant speed. A mode with wavenumber k will grow according to

$$e^{\omega t} \cos kx,$$

where

$$\omega = ku_n - \tau k^3. \tag{24}$$

The pulse initially at s_1 moves to a position s_2 on the finger in a time t given by

$$\sinh 2\pi s_2 = e^{4\pi t} \sinh 2\pi s_1 \tag{25}$$

using (20) with $U = 2$. Let l_1 be a characteristic width of the pulse when it is centred initially at s_1. As it moves backward it dilates to a dimension l_2 according to

$$\frac{l_2}{l_1} = \frac{\mathrm{d}s_2}{\mathrm{d}s_1} = \frac{\tanh 2\pi s_2}{\tanh 2\pi s_1} \tag{26}$$

using (25) and the assumption of small pulse width. The pulse is taken to have the bilaterally symmetric Fourier integral representation

$$f(s,t) = \frac{1}{\pi}\int_0^\infty A(k,t,l_2)\cos ks\,\mathrm{d}k, \tag{27}$$

where s is measured from the instantaneous centre of the convected waveform. The initial spectrum is given by $A(k,0,l_1)$ which evolves to

$$A(k,t,l_2) = A(k,0,l_2)\exp\left(\int_0^\infty \omega(t')\,\mathrm{d}t'\right). \tag{28}$$

Using (22)–(25), the growth factor is found in closed form as

$$\exp\left(\int_0^\infty \omega(t')\,\mathrm{d}t'\right) = \left[\frac{\tanh \pi s_2}{\tanh \pi s_1}\right]^{k/2\pi} \exp\left(-\tau k^3 t\right). \tag{29}$$

Qualitative predictions of the fate of a sufficiently small initial disturbance can now be made using this model. The centre of a disturbance will convect backwards from its initial position in a tip-fixed frame of reference. Ultimately its velocity will become constant, corresponding to the disturbance stopping at a fixed position in laboratory coordinates. At early times the disturbance amplitude will grow but must eventually reach a maximum and then decay. The magnitude of the growth depends on the initial position of the disturbance, becoming large when s_1 is small. During the growth and decay, the width of the disturbed region must increase owing both to the dilation in (26) and also to the earlier decay of the large-wavenumber components as given by the last factor in (29). As an example we calculate the time history of a trapezoidal disturbance of total width 0.06 initially centred at $s_1 = 0.13$ with τ equal to 0.0003. The evolution of the pulse shape, according to (27), is shown in figure 7. For comparison we show, in figure 8, a nonlinear time-dependent calculation with a relatively large pulse introduced at these conditions. As predicted by the linear model, we seen that the disturbance grows rapidly at first but ultimately reaches a limiting height and begins to decay. At the same time the disturbance spreads laterally, assuming a shape that is somewhat similar to those given in figure 7. The central crest of the disturbance is seen to move forward a short distance, in laboratory coordinates, before stopping. The amplitude of the initial bump, 0.003, is much larger than that required to split the finger at this low value of τ. Because it was introduced some distance from the finger tip, it produces only a transient change in finger shape.

The stability of a developed finger in a Hele-Shaw cell can now be re-examined in the light of the numerical and model results presented above. Taylor & Saffman (1959) considered the stability of fully developed fingers for $\tau = 0$ and this work has, more recently, been extended to finite surface tension by McLean & Saffman (1981). In both cases small perturbations to the steady-state solution are assumed to be of the form $\exp(\omega t)$ times a function of the space coordinates. To the extent that (eigen-)

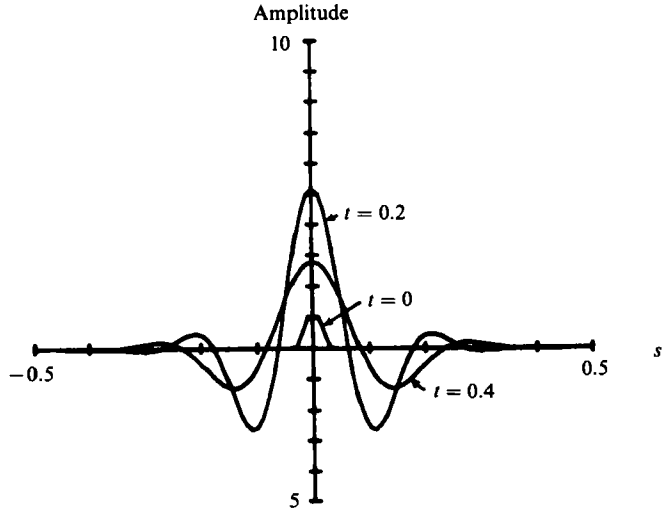

FIGURE 7. The evolution of an initial disturbance on the finger using the simplified linear model. The arclength s is measured from the centre of the disturbance, which is convecting backwards. The amplitude is the perpendicular distance from the undisturbed to the disturbed finger, and t is time.

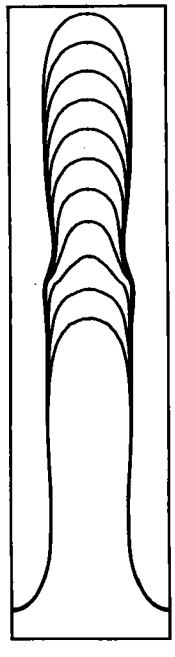

FIGURE 8. The effect of an instantaneously imposed disturbance of amplitude +0.003 on the subsequent development of a finger. The interface curves are presented at time intervals of 0.1. See figure 2(*g*) for comparison with the unperturbed evolution.

solutions of the linearized problem, corresponding to values of ω with positive real part, can be found, the underlying steady-state solution is considered to be unstable. Such eigensolutions were found to exist with or without surface tension. Taylor & Saffman (1959) conclude that the results of their stability analysis are at variance with experiment since apparently steady-state fingers can be produced in the

laboratory without difficulty. In the later paper it is suggested that the resolution of this paradox is associated with the neglect of the variation of the component of interface curvature in the plane perpendicular to the plates of the cell. While this second curvature variation may explain the discrepancy between predicted values of ultimate finger width and the experimental observations (viz Pitts 1980), a simpler explanation would appear to suffice for the stability question. As the present numerical work suggests, a small-amplitude disturbance is convected backwards in a tip-fixed coordinate system. Roughly speaking, the destabilizing influence of the normal component of velocity can only produce a finite alteration of the finger profile, this alteration decreasing as the magnitude of the disturbance decreases. Provided that the disturbance is not large enough to cause the finger to split, it will ultimately decay. The presence or absence of 'instantaneous' instability would appear to be too severe a test. Only if a coordinate system translating with constant velocity could be found in which unstable eigenmodes remain stationary in space can 'operational' linear instability be inferred.

5. Conclusions

Using our nonlinear time-dependent algorithm, we have shown that a stable finger can be formed for a wide range of dimensionless surface-tension values starting from a sinusoidal variation in the interface. Comparing finger widths it is clear that the stable fingers are the same as those obtained by McLean & Saffman (1981) using a steady-state algorithm. For sufficiently large values of surface tension, our results confirm the time-dependent calculations of Tryggvason & Aref (1985) using the 'vortex-in-cell' method.

We have shown that there is no apparent contradiction between our stable fingers and the linear instability found by McLean & Saffman. There are, indeed, disturbances that grow initially, reach a maximum amplitude, and then decay. This type of linear stability analysis can only really prove the stability of a steady-state configuration. A finding of linear instability, though suggestive, can be misleading, as in this case.

We have also shown that the fingers are nonlinearly unstable. In a sense, this is an obvious result. It is clear that a deep notch placed in the tip of the finger will not 'heal' at least for smaller values of dimensionless surface tension. The principal result is that the amplitude of the notch necessary for splitting the finger is very small for small dimensionless surface tension.

We have systematically analysed the effects of recesses and protrusions at various locations on the finger. We find that a recess at the tip has the largest ultimate growth, by far. We have tried large-amplitude disturbances on the side of the finger and we have not been able to grow a vestigial finger on the side. It seems clear, therefore, that a vestigial finger on the side of a growing finger can only be generated by a bifurcation at the tip. One of the resulting fingers becomes suppressed, while the other growing finger centres and expands in the channel, leaving a vestigial finger.

While this paper was under review, our numerical algorithm was generalized by removing the requirement of bilateral symmetry. The resulting simulation of finger motion, for small τ, clearly illustrates the tip-splitting mechanism followed by a period of competition between the two resulting branches with ultimate dominance by one of them. The process repeats as the 'winner' progresses down the channel, leading eventually to a profile with multiple, essentially stagnant, side branches. Further details may be found in DeGregoria & Schwartz (1985). Recent experimental studies at small τ (Park & Homsy 1985 and Nittman *et al.* 1985), provide confirmation for

this process. The fact that finger splitting had not been observed in previous experiments is probably due to the use of narrower cells yielding larger values of τ.

While agreement between computation and experiment is now good at small τ, there is still a significant discrepancy between observed and predicted finger width at large τ-values. This discrepancy is perhaps due to the variation in the radius of curvature in the third dimension with interface speed, as suggested by Pitts (1980). There has also been speculation that the neglect of this effect might account for the discrepancy between experimentally stable fingers, on the one hand, and the linear instability of theoretically computed fingers, on the other hand. The analysis of small disturbances given here seems to indicate that there really is no significant discrepancy after all.

We do not appear to have generated any of the multiple steady-state finger solutions of higher finger width that Romero (1982) or Vanden-Broeck (1983) have found. This may indicate that these other steady-state solutions are significantly less stable than the primary one, or it may simply mean that, starting from a sinusoidal variation in the interface, we achieve the steady-state finger with the smallest width for a given value of surface tension. One way to resolve this issue is to compute the profile for one of these wider steady states, start the time-dependent algorithm in this state, and see if the finger propagates unchanged. We hope to examine this in the near future.

An interesting and potentially important question concerns the stability of developed fingers at very low surface tension. Our heuristic-model calculation in §4 indicates that fingers can be linearly stable. This stability is confirmed by the numerical results for $\tau \geqslant 0.00025$. Finite-amplitude disturbances have been shown to cause tip splitting for larger τ. Thus, linear stability but nonlinear instability is demonstrated for a range of values of τ. Whether fingers remain linearly stable for arbitrarily small τ, or become linearly unstable at a small finite value of τ, is not answerable by us at present. We suspect the former, however, because it provides the simplest explanation consistent with the numerical and experimental results available to date. We have demonstrated that the noise level required to cause tip splitting decreases very rapidly as τ is reduced. Thus tip-splitting may always be expected to occur in Hele-Shaw experiments at high capillary number because some small level of noise is unavoidable. Since the Hele-Shaw model is increasingly being looked upon as a prototype case for studies of pattern formation in other nonlinear systems, the answer to this stability question may have important theoretical implications.

We are happy to acknowledge our indebtedness to Dr Ben White and Professors Greg Baker, Philip Saffman, and George Homsy for useful discussions of the fingering phenomenon.

REFERENCES

BOTHA, J. F. & PINDER, G. F. 1983 *Fundamental Concepts in the Numerical Solution of Differential Equations*. Wiley.

CHOUKE, R. L., VAN MEURS, P. & VAN DER POEL, C. 1959 The instability of slow, immiscible, viscous, liquid–liquid displacements in permeable media. *Trans. AIME* **216**, 188–194.

DEGREGORIA, A. J. & SCHWARTZ, L. W. 1985 Finger breakup in Hele-Shaw cells. *Phys. Fluids* **28**, 2313–2314.

HINDMARSH, A. C., *Livermore Solver for Ordinary Differential Equations* (*LSODE*) Sept. 23, 1980 version, Lawrence Livermore Laboratory, Livermore CA.

JASWON, M. A. & SYMM, G. T. 1977 *Integral Equation Methods in Potential Theory and Elastostatics.* Academic.

JERAUD, J. R., DAVIS, H. T. & SCRIVEN, L. E. 1984 *SPE/DOE Preprint No.* 12691.

MCLEAN, J. W. & SAFFMAN, P. G. 1981 The effect of surface tension on the shape of fingers in a Hele-Shaw cell. *J. Fluid Mech.* **102**, 455–469.

MENG, J. C. S. & THOMSON, J. A. L. 1978 Numerical studies of some nonlinear hydrodynamic problems by discrete vortex element methods. *J. Fluid Mech.* **84**, 433–453.

NITTMANN, J., DACCORD, G. & STANLEY, H. E. 1985 Fractal growth of viscous fingers: quantitative characterization of a fluid instability phenomenon. *Nature* **314**, 141–144.

PARK, C.-W. & HOMSY, G. M. 1984 Two-phase displacement in Hele-Shaw cells: theory. *J. Fluid Mech.* **139**, 291–308.

PARK, C.-W. & HOMSY, G. M. 1985 The instability of long fingers in Hele-Shaw flows. *Phys. Fluids* **28**, 1583–1585.

PATERSON, L. 1981 Radial fingering in a Hele-Shaw cell. *J. Fluid Mech.* **113**, 513–529.

PETERS, E. J. & FLOCK, D. L. 1981 The onset of instability during two-phase immiscible displacement in porous media. *SPE J.* **21**, 249–258.

PITTS, E. 1980 Penetration of fluid into a Hele-Shaw cell: the Saffman–Taylor experiment. *J. Fluid Mech.* **97**, 53–64.

RESHOTKO, E. 1976 Boundary-layer stability and transition. *Ann. Rev. Fluid Mech.* **8**, 311–348.

ROMERO, L. 1982 Ph.D. thesis, California Institute of Technology.

SAFFMAN, P. G. & TAYLOR, G. I. 1958 The penetration of a fluid into a porous medium or Hele-Shaw cell containing a more viscous liquid. *Proc. R. Soc. Lond.* A **245**, 312–329.

TAYLOR, G. I. & SAFFMAN, P. G. 1959 A note on the motion of bubbles in a Hele-Shaw cell and porous medium. *Q. J. Mech. Appl. Maths* **12**, 265–279.

TRYGGVASON, G. & AREF, H. 1983 Numerical experiments on Hele-Shaw flow with a sharp interface. *J. Fluid Mech.* **136**, 1–30.

TRYGGVASON, G. & AREF, H., 1985 Finger interaction mechanisms in stratified Hele-Shaw flow. *J. Fluid Mech.* **154**, 287–301.

VANDEN-BROECK, J. M. 1983 Fingers in a Hele-Shaw cell with surface tension. *Phys. Fluids* **26**, 2033–34.

WEHAUSEN, J. & LAITONE, E. 1960 Surface waves. *Handbuch der Physik*, vol. 9 (ed. S. Flügge), pp. 446–778.